Title

S100A10 Is a Critical Mediator of GAS6/AXL-Induced Angiogenesis in Renal Cell Carcinoma.

Journal

Cancer Research, 79(22)

Authors

Xiao, Yiren
Zhao, Hongjuan
Tian, Lei
et al.

Publication Date

2019-11-15

DOI

10.1158/0008-5472.CAN-19-1366

Peer reviewed

Published in final edited form as:

Cancer Res. 2019 November 15; 79(22): 5758–5768. doi:10.1158/0008-5472.CAN-19-1366.

S100A10 is a critical mediator of GAS6/AXL-induced angiogenesis in renal cell carcinoma

Yiren Xiao[1,*], **Hongjuan Zhao**[2,*], **Lei Tian**[3], **Rosalie Nolley**[2], **Anh N. Diep**[1], **Anne Ernst**[1], **Katherine C. Fuh**[4], **Yu Rebecca Miao**[1], **Rie von Eyben**[1], **John T. Leppert**[2], **James D. Brooks**[2], **Donna M. Peehl**[2], **Amato J. Giaccia**[1], **Erinn B. Rankin**[1,5,**]

[1]Department of Radiation Oncology, Stanford University, Palo Alto, CA 94305

[2]Department of Urology, Stanford University, Palo Alto, CA 94305

[3]Department of Medicine, Division of Cardiology, Stanford University, Palo Alto, CA 94305

[4]Department of Obstetrics and Gynecology, Washington University, St. Louis, MO 63110

[5]Department of Obstetrics and Gynecology, Stanford University, Palo Alto, CA 94305

Abstract

Angiogenesis is a hallmark of cancer that promotes tumor progression and metastasis. However, antiangiogenic agents have limited efficacy in cancer therapy due to the development of resistance. In clear cell renal cell carcinoma (ccRCC), AXL expression is associated with antiangiogenic resistance and poor survival. Here, we establish a role for GAS6/AXL signaling in promoting the angiogenic potential of ccRCC cells through the regulation of the plasminogen receptor S100A10. Genetic and therapeutic inhibition of AXL signaling in ccRCC tumor xenografts reduced tumor vessel density and growth under the renal capsule. GAS6/AXL signaling activated the expression of S100A10 through SRC to promote plasmin production, endothelial cell invasion and angiogenesis. Importantly, treatment with the small molecule AXL inhibitor cabozantinib or an ultra-high affinity soluble AXL Fc fusion decoy receptor (sAXL) reduced the growth of a pazopanib-resistant ccRCC patient-derived xenograft. Moreover, the combination of sAXL synergized with pazopanib and axitinib to reduce ccRCC patient-derived xenograft growth and vessel density. These findings highlight a role for AXL/S100A10 signaling in mediating the angiogenic potential of ccRCC cells and support the combination of AXL inhibitors with antiangiogenic agents for advanced ccRCC.

Keywords

Tumor microenvironment; endothelial cells; kidney cancer; von Hippel Lindau; angiogenesis; AXL; plasmin; S100A10

**Correspondence should be addressed to: Erinn B. Rankin (erankin@stanford.edu), 269 Campus Drive, 1245 CCSR, Stanford, CA 94305, Tel: 650-497-8742.

*These authors contributed equally to the work.

Conflict of Interest Statement: Dr. Amato Giaccia is a shareholder for the company Aravive that has a soluble AXL receptor Fc fusion protein in clinical trials. Drs. Giaccia, Rankin, Fuh and Miao hold patents at Stanford University for Inhibition of AXL signaling in anti-metastatic therapy (US Patent PCT/US2011/022125) and Modified AXL peptides and their use in inhibition of AXL signaling in anti-metastatic therapy (US Patent PCT/US2013/074786).

Introduction

Renal cell carcinoma is a common malignancy with 403,262 new cases and 175,098 deaths worldwide in 2018 (1). Clear cell renal cell carcinoma (ccRCC) is the most common form of kidney cancer and is associated with loss of the von Hippel Lindau (*VHL*) tumor suppressor. *VHL* loss results in the constitutive activation of the hypoxia inducible transcription factors (HIF-1 and HIF-2) and their targets, including the proangiogenic factors VEGF and PDGF (2). As a result, RCC tumors are highly vascularized and initially respond to antiangiogenic therapies, including tyrosine kinase inhibitors (TKI) (3). While antiangiogenic therapy has significantly increased progression-free survival in patients with advanced renal cancer, the majority of patients treated with these agents eventually become resistant and progress (4,5). Thus, antiangiogenic drug resistance is a major challenge in the clinical management of renal cell carcinoma. Multiple mechanisms of acquired resistance to antiangiogenic agents have been proposed in ccRCC including the activation of compensatory angiogenesis mechanisms and increased tumor invasion (6,7). The identification of druggable TKI resistance mechanisms in ccRCC are needed to improve the overall survival rate of patients with advanced kidney cancer.

The receptor tyrosine kinase, AXL, has emerged as an important therapeutic target in cancer that is associated with both metastatic and drug resistant phenotypes of advanced tumors. Moreover, multiple AXL inhibitors have advanced to clinical studies, highlighting the translational potential of targeting AXL signaling for cancer therapy (8-10). In ccRCC, AXL is a direct target of VHL/HIF signaling and its expression correlates with the lethal phenotype (11-13). Moreover, AXL expression is increased in sunitinib treated ccRCC patient tumors (14). The majority of AXL activation in ccRCC cells occurs in a ligand-dependent manner mediated by GAS6 (11). In cancer, GAS6/AXL signaling can be activated in an autocrine or paracrine manner with tumor cells as well as cells within the tumor microenvironment, including macrophages and endothelial cells producing biologically relevant sources of GAS6 (15). Analysis of GAS6 expression and AXL activation in a panel of ccRCC cells revealed that both autocrine and paracrine mechanisms are responsible for activation of AXL in these cells (11). While GAS6/AXL signaling is known to promote the invasive and metastatic potential of tumor cells, the role of GAS6/AXL signaling in regulating the angiogenic potential of tumor cells is not known (11-13).

In this report, we establish a role for GAS6/AXL signaling in promoting the angiogenic potential of ccRCC cells through the regulation of S100A10. Genetic inhibition of AXL in ccRCC cells reduced tumor vessel density and growth under the renal capsule. RNA sequencing analysis of AXL wild type and AXL deficient cells revealed that AXL promotes the expression of the plasminogen receptor S100A10. We demonstrate that the proangiogenic factor S100A10 is increased in ccRCC cells through AXL/SRC signaling. Moreover, S100A10 in ccRCC cells is sufficient to promote AXL-mediated plasmin production, endothelial invasion and angiogenesis. In ccRCC patients, S100A10 expression correlates with AXL expression. Finally, therapeutic blockade of GAS6/AXL signaling reduced ccRCC and patient derived xenograft tumor vessel density and growth in the kidney.

Our findings identify GAS6/AXL signaling as an important pathway driving ccRCC angiogenesis and have important therapeutic implications for the treatment of advanced renal clear cell carcinoma.

Materials and Methods

Cell Lines and Culture Conditions

786-O and M62 cells were maintained in Dulbecco's modified Eagle medium (DMEM) supplemented with 10% FBS. HUVEC (ATCC® CRL-1730) cells were purchased from ATCC and cultured in endothelial culture medium (CC-3156, LONZA) supplemented with Growth Medium 2 Supplement (C-39211, PromoCell). The M62 clear cell carcinoma cell line was a generous gift from Jose Karam and colleagues (MD Anderson, Houston (16)). For hypoxia treatments, cells were plated at the desired density 12 h before placement in a hypoxia chamber (Invivo2-400; Ruskin Technologies) maintained at 2% oxygen for 0–72 h, depending on the experiment. The M62 cell line expresses endogenous GAS6 whereas the 786-0 cell line does not express endogenous GAS6 (11). Therefore, for all in vitro experiments, cells were pretreated with 200ng/mL of recombinant human GAS6 (carrier free, 885-GS-050; R&D Systems) with >90% purity and <1.0 EU/1 μg of endotoxin for 24 hours before plating into the individual in vitro assays described below.

All cell lines were authenticated from the original source and were used within 6 months of receipt. Additionally, cells were tested upon receipt for viability, cell morphology and the presence of *Mycoplasma* and viruses (Charles River Laboratories).

Conditioned Media

Forty-eight hours after transfection of ccRCC cells, the cells were treated with 200 ng/ml of GAS6 in serum free medium for 24 hours. The medium was collected and centrifuged at 12,000g for 10 min. The supernatant was used for the HUVEC matrigel invasion and in vivo matrigel plug assays.

Correlation of Transcript Levels of AXL, ANXA2 and S100A10 in ccRCC Patient Samples

Gene expression profile of a cohort of 76 ccRCC patients were retrieved from Gene Expression Onmbus (GEO) (GSE36985). Expression levels of *AXL*, *ANXA2* and *S100A10* were extracted and log2 transformed in Excel. Log2 transformed expression levels were then centered and scatter plot was generated in Excel. Person's correlation coefficient was calculated in Prism 6.

The Cancer Genome Atlas Data Analysis

The cBio Cancer Genomic Portal was used to analyze *AXL*, *S100A10* and *ANXA2* expression and survival in the Kidney Renal Clear Cell Carcinoma dataset (17). Consensus cluster analysis was performed using ConsensusClusterPlus (18).

shRNA and siRNA

Oligos for *AXL* shRNA were synthesized as previously described (11). For more details please see the Supplementary Methods section.

Immunohistochemistry

The primary antibodies used for IHC staining are AXL (1:100, AF154, R&D), S100A10 (1:200, 4E7E10, Santa Cruz), CD31 (1:200, ab28364, ABcam), Ku70 (1:200, AB18560, ABcam), CAIX (1:500, NB-100-417, Novus), CD117 (1:200, CME296, Biocare Medical), CD10 (1:200, CM129AK, Biocare Medical) and CK7 (1:200, OV-TL 12/30, Dako Agilent). For more details please see Supplementary Methods section.

Real-time PCR

RNA was isolated using Trizol (Invitrogen) and subsequently treated with DNase I (Thermo). First-strand cDNA synthesis was performed with SuperScript II Reverse Transcriptase and random primers (Applied Biosystems) according to the manufacturer's instructions. Quantitative real-time PCR was carried out using Power SYBR Green Master Mix (Bio-rad), detection and data analysis were executed with the 7900HT Fast Real-Time PCR System (Applied Biosystems) by computing the results relative to a standard curve made with cDNA pooled from all samples, normalized to 18S. For more details and primer sequences please see Supplementary Methods section.

Recombinant Protein Production

The soluble AXL (sAXL) Fc fusion proteins were generated as previously described (19). The sAXL (AVB500) was kindly provided by ARAVIVE Inc and is currently being tested in Phase !b clinical trials.

Plasminogen Activity Assay

The kinetics of cell-mediated plasminogen activation was determined by measuring amidolytic activity of the plasmin generated from plasminogen (20). Cells (1×10^4) were seeded on 96-well culture plates and stimulated with 200ng/mL of recombinant human GAS6 in serum free media overnight. Cells were washed with PBS and incubated with plasmin substrate (V0882, Sigma) at a final concentration of 100 μM in phenol red-free and serum free DMEM. The reaction was initiated by the addition of 0.5 μM [Glu]-plasminogen (528180, EMD Millipore) to the cells. The rate of plasmin production was measured at 405 nm with Perkin Elmer HTS 7000 Bioassay reader (Shelton, CT, USA) at indicated time point.

Matrigel Invasion

HUVEC cells were cultured in endothelial culture medium (CC-3156, LONZA) supplemented with Growth Medium 2 Supplement (C-39211, PromoCell). Matrigel invasion chambers with 8.0 μm pore polyester membrane were primed with 500 μl of cancer cell conditioned media overnight in 37°C CO_2 incubator. 5×10^4 HUVEC cells in 500 μl of endothelial basal culture medium were plated on top of the control inserts or matrigel invasion inserts and 750 μl of endothelial culture medium supplemented with Growth Medium 2 Supplement was filled in the bottom of the inserts. Invasion and control inserts were stained and analyzed 16 h later. Percent invasion through the matrigel was normalized to the average number of cells that migrated through the control inserts.

Protein Isolation and Western Blot Analysis

Protein lysates were harvested in 9M Urea, 0.075M Tris buffer (pH7.6). Protein lysates were quantified using the using BCA Protein Assay kit (Pierce), and 50–100 μg of protein was subjected to reducing SDS/PAGE using standard methods, then transferred onto 0.2 μm supported nitrocellulose membranes (Bio-Rad Laboratories). Western blots were probed with antibodies against AXL (1:1000, AF154, R&D Systems); p-AXL (1:1000, D12B2, Cell Signaling Technology), SRC (1:1000, 32G6, Cell Signaling Technology), p-SRC (1:1000, CAT#:2105, Cell Signaling Technology); S100A10 (1:1000, 4E7E10, Santa Cruz), ANXA2 (1:1000, CAT#: NBP1-31310, Novus Biologicals), HSP70 (1:1000, H5147, Sigma Aldrich). Secondary antibodies used in this study were HRP-conjugated anti-goat (1:50,000; sc-2020, Santa Cruz), HRP-conjugated anti-mouse (1:5000; 7076P2, Cell Signaling Technology) or HRP-conjugated anti-rabbit (1:5000; 7074P2, Cell Signaling Technology). Immunoblots were developed with SuperSignal West Dura Extended Duration Substrate (Thermo Fisher Scientific) and visualized with ChemiDoc XRS+ imaging system equipped with Image Lab Software (Bio-Rad Laboratories).

For GAS6 stimulation, cells were serum deprived for 48 h. Cells were then pretreated with PP2 (500 nM) or dasatinib (50 nM) for 2 hours followed by addition of GAS6 (200 ng/mL) for 4 hours.

In vivo Matrigel Plug Assay

All procedures involving animals and their care were approved by the Institutional Animal Care and Use Committee of Stanford University in accordance with institutional and National Institutes of Health guidelines. Six to eight-week-old $Rag2^{-/-}IL2rg^{-/-}$ double knockout mice were used for the in vivo plug assay. Growth factor reduced matrigel (250 μL) was mixed with 250 μL of conditioned media (CM) from ccRCC cells described above and subcutaneously injected into the mice. After 10 days, matrigel plugs were analyzed for angiogenesis by macroscopic evaluation, histological analysis and quantified by analyzing hemoglobin content with Drabkin reagent (Sigma-Aldrich). For hemoglobin analysis, matrigel plugs were dissected and weighed before proceeding. Then the matrigel was transferred to an eppendorf tube containing 0.5 ml of de-ionized water. After overnight incubation at 37 °C, lysates were centrifuged at 12,000xg for 10 min to remove tissue pieces and gel. The supernatant was used for hemoglobin quantification with the Drabkin assay according to manufacturer's instructions. The final result was normalized to the initial matrigel weight.

Tumor Xenografts

To establish orthotropic ccRCC xenograft model, $Rag2^{-/-}IL2rg^{-/-}$ double knockout mice aged from 6 and 12 weeks were injected with a 100 μL of collagen plug (BD Bioscience) containing 1×10^6 ccRCC cells under the renal capsule as previously described (21). For more details please see Supplementary Methods.

Patient Derived Xenografts

All patients who participated in this study provided written informed consent for collection and research use of their materials and use of these samples was approved by the Stanford

University Institutional Review Board (IRB #34175) in accordance with recognized ethical guidelines per the U.S. Common Rule. Patient derived tissue RCC054 was obtained from a 44-year-old male undergoing surgery to remove metastatic RCC tissue from the colon at Stanford under an institutional review board–approved protocol with informed consent. We established two additional RCC PDX models from materials received from the NCI Patient-Derived Models Repository (PDMR), NCI-Frederick, Frederick National Laboratory for Cancer Research, Frederick, MD. URL – http://www.pdmr.nci.gov. For more details please see Supplementary Methods

Drug Administration

Pazopanib (LC Laboratories, MA) was prepared in 0.5% hydroxypropylmethyl cellulose and 0.1% Tween-80. Axitinib (LC Laboratories, MA) was prepared in 0.5% carboxymethyl cellulose (PH=2). Cabozantinib (LC Laboratories, MA) was formulated in sterile saline/10 mmol/L HCl. Mice were administered 0.1 mL of pazopanib (30mg/kg/day for RCC054, NCI597326 and NCI961994), axitinib (36mg/kg/day for NCI961994), cabozantinib (10mg/kg/day for RCC054 and M62) or vehicle by oral garage. For sAXL experiments, mice were treated with control (saline) or sAXL therapy at 20 mg/kg every two days by i.p. injection.

RNA-Sequencing and Data Analyses

RNA samples were extracted from 1×10^6 cancer cells using Qiagen RNeasy Mini Kit. Two μg /sample were delivered to Novogene Corporation for cDNA library preparation and sequencing. Briefly, cDNA was sonicated and subjected to library preparation using the Illumina TruSeq DNA sample preparation kit. Total RNA from 786-O-sh*SCM1,* 786-O-sh*AXL1,* M62-sh*SCM1* and *M62*-sh*AXL1* cell were used for the preparation of RNA-Seq libraries with Illumina's TruSeq RNA Library Prep Kit v2 according to manufacturer's protocol. Sequencing was performed on Illumina HiSeq 2000. For more details please see Supplementary Methods.

Statistical Analysis

Continuous outcomes were analyzed using a t test when comparing two groups. Continuous outcomes were analyzed in an ANOVA model when comparing more than two groups. Pair-wise post hoc testing was done using a Tukey adjustment for multiple comparisons. Repeated measures outcomes were analyzed in a mixed effects model to account for the within mouse correlations. Time to event outcomes were summarized using Kaplan-Meier curves and groups were compared using log-rank tests. The rate of plasmin generation in figures 4a-d were modeled using a four-parameter dose response curve. The four-parameter dose response curves and the t tests were performed in Prism v 8.0.1 (GraphPad Software Inc., San Diego, CA). All other analyses were performed in SAS v9.4 (SAS Institute Inc., Cary, NC). All tests were two-sided with an alpha of 0.05.

Results

Genetic inhibition of AXL in ccRCC cells reduces tumor vessel density and growth.

To investigate the role of AXL in regulating the angiogenic potential of ccRCC cells *in vivo*, we first utilized a genetic approach to knock down *AXL* expression in two *VHL* deficient ccRCC cell lines (786-O and M62, (16)). Endogenous *AXL* expression in both ccRCC cell lines was significantly repressed by the *AXL* shRNA targeting sequences relative to the control shRNA sequences (Supplementary Fig. S1A-B, (11,22)). No significant differences in tumor cell proliferation or survival were observed when comparing the growth of AXL knockdown or control cell lines under normoxic or hypoxic conditions *in vitro* (Supplementary Fig. S1C-H). In contrast, primary ccRCC tumor growth under the renal capsule was significantly impaired in mice injected with AXL knockdown tumor cells compared to mice injected with AXL wild type shSCM cells (Fig. 1A-D). Both histologic analysis and quantification of CD31 positive blood vessels revealed that tumor vessel density was significantly reduced in AXL knockdown tumors compared to AXL wild type ccRCC tumors (Fig. 1E-F). These findings demonstrate that AXL is an important factor governing ccRCC tumor vascular density and growth at the kidney, suggesting a role for AXL in mediating the angiogenic potential of ccRCC cells.

AXL promotes S100A10 expression in ccRCC cells through SRC family kinase activity.

To identify proangiogenic programs regulated by AXL in ccRCC cells, we performed RNA sequencing (RNA-seq) based gene expression profiling of two independent AXL wild type and AXL knockdown ccRCC cells. Direct pairwise comparison of AXL wild type and AXL knockdown cells revealed hundreds of genes whose expression was changed more than 2-fold in AXL knockdown cells compared to AXL wild type cells (Fig. 2A, Supplementary Table 1-2). Forty-two genes were significantly altered (upregulated or downregulated) in both the 786-O and M62 cell lines (Fig. 2A, Supplementary Table 3). Of the 42 genes, 10 genes were significantly decreased upon AXL knockdown (Fig. 2B, Supplementary Table 4). Notably, the expression of the plasminogen receptor *S100A10*, was reduced greater than 2-fold in shAXL 786-O and M62 cells compared to shSCM 786-O and M62 cells (Fig. 2B). The S100A10-annexin II plasminogen receptor complex has been shown to enhance the formation of plasmin to promote ECM degradation, neovascularization, invasion, metastasis and drug resistance (23-25). In addition to *S100A10*, *Annexin A2* (*ANXA2*) expression was reduced >1.7 fold in both AXL knockdown cell lines compared to control lines (Fig. 2B). In human ccRCC samples, *AXL* expression correlates with *S100A10* and increased *S100A10* expression independently correlates with poor patient survival in ccRCC patients (Fig. 2C and 2D). Additionally, *AXL* expression correlates with *ANXA2* and increased *ANXA2* expression independently correlates with poor patient survival in ccRCC patients indicating that the S100A10/ANXA2 plasminogen pathway may contribute to ccRCC tumor progression (Fig. 2E and 2F).

We next confirmed AXL-dependent regulation of *S100A10* and *ANXA2* at the mRNA and protein level in 786-O and M62 ccRCC cells. Genetic inactivation of *AXL* significantly reduced *S100A10* mRNA and protein as determined by real time PCR and western blot analyses respectively (Fig. 2G-I, Supplementary Fig. S2A-C). While AXL inactivation

reduced *ANXA2* at the mRNA level, ANXA2 total protein levels were not consistently reduced in AXL knockdown cells relative to the shSCM cells (Supplementary Fig. S2D-G). Therefore, we sought to further investigate the regulation and functional role of S100A10 in AXL positive ccRCC cells. GAS6-mediated activation of AXL signaling increased *S100A10* mRNA and protein expression (Fig. 2J-K). Previous studies have shown that growth factor receptor signaling mediated by transforming growth factor-B, epidermal growth factor, or basic fibroblast growth factors can increase S100A10 expression through a variety of downstream signaling pathways (for review (26)). In kidney cancer, we recently reported that GAS6/AXL signaling is a potent activator of SRC activity (11). To determine whether GAS6-mediated S100A10 expression occurs through the activation of SRC, we utilized the SRC family kinase inhibitors PP2 and dasatinib. Pretreatment with PP2 or dasatinib abolished the GAS6 mediated increase in SRC phosphorylation as well as S100A10 expression (Fig. 2J-K). These data suggest that SRC family kinase signaling is involved in the induction of S100A10 by GAS6/AXL signaling in ccRCC cells.

AXL and S100A10 promote ccRCC plasmin production and promote angiogenic processes *in vitro* and *in vivo*.

Our findings above identify AXL signaling in the regulation of S100A10 expression. Normal cells and cancer cells utilize S100A10 to convert plasminogen to plasmin at the cell surface (26). Therefore, we compared the rates of plasmin generation between AXL deficient and AXL wild type ccRCC cells. Using an *in vitro* assay that measures the conversion of plasminogen to plasmin, we found that the rate of plasmin generation was significantly reduced in shAXL knockdown ccRCC (786-O and M62 cells) compared to shSCM cells (Supplementary Fig. S3A-B). Similarly, we utilized a siRNA approach to directly compare plasminogen conversion between AXL and S100A10 knockdown cells (Fig. 3A-B). Compared to the siControl treated cells, both siAXL and siS100A10 knockdown cells exhibited reduced rates of plasmin production (Fig. 3C-D). These findings demonstrate that both AXL and S100A10 in ccRCC cells promote plasmin production from plasminogen.

Plasmin production can facilitate angiogenesis through multiple mechanisms. Plasmin is an enzyme that activates matrix metalloproteinases to degrade fibrin, fibronectin, laminin and collagen within the extracellular matrix (ECM). The proteolytic breakdown of the ECM facilitates endothelial cell invasion as well as releases proangiogenic factors sequestered within the matrix (27-29). We examined whether the conditioned media from siAXL or siS100A10 ccRCC cultures affected endothelial (HUVEC) invasion compared to siControl conditioned media. HUVEC invasion through matrigel, an extracellular basement membrane matrix, primed with conditioned media from siAXL or siS100A10 treated ccRCC tumor cells was significantly reduced compared to matrigel inserts primed with siControl ccRCC media (Fig. 3E-F). These findings demonstrate that secreted factors regulated by AXL and S100A10 in ccRCC cells are sufficient to prime matrigel matrix substrates to enhance endothelial cell invasion *in vitro*.

We next investigated the role of AXL and S100A10 in regulating the angiogenic potential of ccRCC conditioned media in vivo using a matrigel plug assay (30). $Rag2^{-/-}IL2rg^{-/-}$ mice

were injected subcutaneously with matrigel containing supernatant from siControl, siAXL, or siS100A10 treated ccRCC cells. After 10 days, matrigel plugs were harvested and hemoglobin concentration was quantified. The hemoglobin concentration of matrigel plugs containing siAXL and siS100A10 conditioned media was reduced (5-fold) compared to matrigel plugs containing siControl conditioned media (Fig. 3G-H). These findings demonstrate that AXL and S100A10 promote the angiogenic potential of ccRCC cells *in vivo*.

To determine if S100A10 is a key factor promoting the angiogenic potential of ccRCC cells mediated by AXL signaling. For this purpose, S100A10 expression was rescued with an exogenous expression vector in AXL knockdown ccRCC cells (Fig. 3I). The addition of S100A10 expression restored plasminogen to plasmin conversion, HUVEC invasion and angiogenesis in the matrigel plug assay of shAXL ccRCC cells to levels that were comparable to the shSCM control cells indicating that S100A10 is an important factor driving the angiogenic potential of ccRCC cells downstream of AXL signaling (Fig. 3J-L).

Therapeutic inhibition of GAS6/AXL signaling inhibits ccRCC tumor growth and synergizes with pazopanib in ccRCC patient derived xenografts.

The results above identify an important role for AXL signaling in mediating ccRCC tumor growth and angiogenesis, raising the intriguing possibility that AXL inhibitors may be effective in blocking ccRCC tumor progression at multiple tissue sites when utilized alone or in combination with antiangiogenic agents. In support of this notion, cabozantinib, a small-molecule TKI that targets VEGFR, MET and AXL has shown significant responses in kidney cancer (31) Cabozantinib is approved by the Food and Drug Administration (FDA) and the European Medicines Agency (EMA) as a first-line therapy in patients with advanced RCC. We first evaluated the efficacy of cabozantinib in ccRCC tumor cell xenograft. Cabozantinib treatment (10mg/kg) significantly reduced the tumor growth of the ccRCC M62 tumor xenografts (Supplementary Fig. S4). These findings are consistent with previous reports of cabozantinib reducing tumor growth and angiogenesis (14,32). We next sought to determine if selective inhibition of AXL signaling is sufficient to inhibit tumor growth and angiogenesis. For this purpose we have developed a highly potent, selective and safe GAS6/AXL inhibitor by generating a soluble AXL decoy receptor that is fused to human IgG1 (sAXL, (19)). To determine the efficacy of sAXL in ccRCC tumor progression, we treated mice with established 786-O or M62 tumors under the renal capsule or liver a common ccRCC metastatic site. Soluble AXL treatment (20 mg/kg, every two days) resulted in a significant reduction of tumor growth at both the liver and kidney compared to the vehicle treatment (Fig. 4A-D). Reduced tumor growth in the sAXL treated ccRCC xenografts in the kidney and liver was associated with a reduction in tumor vessel density (Fig. 4E-F).

We next evaluated the efficacy of AXL targeting agents in ccRCC patient derived xenografts (PDXs). We established a PDX line (RCC054) from a ccRCC patient with colon metastases. This patient, a 44-year-old male, received radical nephrectomy surgery upon initial diagnosis. Three months after surgery, the patient developed lung metastases and was treated with pazopanib. The patient progressed on pazopanib and one year later developed colon

metastases (Supplementary Fig. S5A). Tissue was collected from the metastatic colon lesion and tissue slice grafts and PDX lines were generated using our previously established methods (21). Histological analysis of the patient tumor demonstrated that histological features of clear cell renal cell carcinoma as well as expression of ccRCC markers including Ku70, CAIX, CD10 and Pax8 (Fig. 5A, (33)). Moreover, histological and immunohistochemical analysis of the PDX tumor showed that the PDX tumor maintained the ccRCC phenotype and expressed AXL as well as S100A10 (Fig. 5A). Sequencing analysis of the PDX tissue revealed a deletion within VHL at position 492 (Fig. 5B). Pazopanib treatment did not significantly affect tumor progression in this PDX line (RCC054) when treatment began either early (7 days-post tissue implantation) or with established disease (14 days post implantation, Fig. 5C-G). In contrast, cabozantinib treatment (10 mg/kg) significantly reduced the growth of RCC054 (Fig. 5C). Moreover, single agent sAXL therapy as well as the sAXL and pazopanib combination therapy significantly reduced the growth of RCC054 when treatment began at the early stage at 7 days following tumor implantation (Fig 5D). The decrease in tumor growth mediated by sAXL therapy and the sAXL+pazopanib therapy was associated with a decrease in tumor vessel density (Fig. 5E). Importantly, sAXL therapy synergized with pazopanib when used to treat established disease in multiple VHL deficient ccRCC PDX models (Fig. 5F-H, Supplementary Fig.S5B-F). We also observed that sAXL therapy synergized with the TKI axitinib, in ccRCC PDX NCI961994 (Fig. 5H). These findings demonstrate that AXL inhibition is sufficient to inhibit ccRCC tumor progression and vessel density in ccRCC tumor xenografts and PDX models.

Discussion

Our studies reveal a role for the receptor tyrosine kinase AXL in promoting the angiogenic potential and growth of ccRCC cells. We demonstrate that genetic and therapeutic inactivation of AXL in ccRCC cells is sufficient to reduce tumor vessel density and growth at the kidney. AXL-mediated tumor growth is not associated with an intrinsic regulation of tumor proliferation or survival but rather regulation of the angiogenic potential of ccRCC cells. Previous studies linking AXL to angiogenesis have shown that AXL expression in endothelial cells promotes proangiogenic processes including endothelial migration, proliferation and tube formation (34-37). One mechanism by which AXL signaling on endothelial cells promotes proangiogenic functions is through the regulation of VEGF-A-mediated PI3K/Akt signaling (38). Our study identifies an important role for AXL signaling in ccRCC tumor epithelial cells in the regulation of angiogenic processes including endothelial cell invasion.

We define a pathway by which GAS6/AXL signaling promotes the angiogenic potential of ccRCC cells through the activation of the S100A10/plasmin pathway. The plasminogen receptor S100A10 plays an important role in plasmin production by endothelial cells, macrophages and cancer cells. S100A10-deficient mice exhibit reduced fibrinolysis in response to batroxobin-induced vascular thrombi and have reduced macrophage recruitment in response to inflammatory stimuli (24,39). Moreover, S100A10 deficient endothelial cells have impaired neovascularization in matrigel plugs in vivo associated with reduced tumor growth and vascular density suggesting a role for S100A10 in angiogenesis (24,40). In

cancer cells, S100A10 expression is increased relative to normal tissue where it promotes tumor migration, invasion and metastasis (for a recent review (41)). *S100A10* gene expression can be induced by signaling events mediated through IFN-gamma, glucocorticoids, TGF-B, gonadotropin, EGF, bFGF, and interleukin 1B. Additionally, ANXA2 has been shown to regulate S100A10 mRNA and protein stability (for a recent review (26)). Our study demonstrates that S100A10 expression can be induced by GAS6/AXL signaling in an SRC dependent manner to promote the angiogenic and invasive potential of ccRCC cells. Previous reports have shown that S100A10 is increased in renal cell carcinoma relative to normal tissue (42,43). We demonstrate that elevated *S100A10* correlates with poor survival in ccRCC patients, suggesting S100A10 may be an important factor in the pathogenesis of ccRCC. Future studies are needed to define the role of S100A10 in ccRCC tumor growth, metastasis and TKI resistance.

Our study has important therapeutic implications for the treatment of advanced ccRCC. Kidney cancer is among the top 10 most common cancers in men worldwide (1). While antiangiogenic therapy has increased disease free progression and survival in patients with advanced kidney cancer, the majority of patients eventually progress and succumb to metastatic disease (44). Mechanisms of angiogenic resistance include activation of compensatory angiogenesis pathways as well as increased tumor invasion (6,7). Our data demonstrate that AXL promotes the angiogenic potential of ccRCC cells in vitro and in vivo. Moreover, we found that treatment with the AXL targeting agents cabozantinib or soluble AXL decoy therapy can reduce tumor growth and vascularization in ccRCC tumor xenografts and PDX models. We report that selective inhibition of AXL using the sAXL decoy receptor was sufficient to reduce tumor growth as a single agent therapy and synergize with pazopanib or axitinib in ccRCC PDX models. Our data are supported by a recent publication demonstrating that AXL expression is increased in sunitinib resistant ccRCC patients (14). Overall, our data suggest that anti-AXL therapy may be an effective and safe strategy to prevent and treat pazopanib resistant disease and provide preclinical data to support the rationale combination of AXL inhibitors with antiangiogenic agents for the treatment of advanced kidney cancer.

Supplementary Material

Refer to Web version on PubMed Central for supplementary material.

Acknowledgments

This work was supported by NIH Grants CA-198291 (AJG and EBR) and the My Blue Dots Fund (EBR). This work was supported by the Deutsche Forschungsgemeinschaft (DFG, ER 9061-1, AE).

References

1. Bray F, Ferlay J, Soerjomataram I, Siegel RL, Torre LA, Jemal A. Global cancer statistics 2018: GLOBOCAN estimates of incidence and mortality worldwide for 36 cancers in 185 countries. CA Cancer J Clin 2018;68:394–424. [PubMed: 30207593]
2. Rankin EB, Giaccia AJ. The role of hypoxia-inducible factors in tumorigenesis. Cell Death Differ 2008;15:678–85. [PubMed: 18259193]

3. Motzer RJ, Hutson TE, Cella D, Reeves J, Hawkins R, Guo J, et al. Pazopanib versus sunitinib in metastatic renal-cell carcinoma. The New England journal of medicine 2013;369:722–31. [PubMed: 23964934]
4. Li L, Kaelin WG Jr. New insights into the biology of renal cell carcinoma. Hematol Oncol Clin North Am 2011;25:667–86. [PubMed: 21763962]
5. Rini BI. Metastatic renal cell carcinoma: many treatment options, one patient. Journal of clinical oncology : official journal of the American Society of Clinical Oncology 2009;27:3225–34. [PubMed: 19470934]
6. Bergers G, Hanahan D. Modes of resistance to anti-angiogenic therapy. Nature reviews Cancer 2008;8:592–603. [PubMed: 18650835]
7. Siska PJ, Beckermann KE, Rathmell WK, Haake SM. Strategies to overcome therapeutic resistance in renal cell carcinoma. Urologic oncology 2017;35:102–10. [PubMed: 28089416]
8. Rankin EB, Giaccia AJ. The Receptor Tyrosine Kinase AXL in Cancer Progression. Cancers 2016;8
9. Scaltriti M, Elkabets M, Baselga J. Molecular Pathways: AXL, a Membrane Receptor Mediator of Resistance to Therapy. Clinical cancer research : an official journal of the American Association for Cancer Research 2016;22:1313–7. [PubMed: 26763248]
10. Graham DK, DeRyckere D, Davies KD, Earp HS. The TAM family: phosphatidylserine sensing receptor tyrosine kinases gone awry in cancer. Nature reviews Cancer 2014;14:769–85. [PubMed: 25568918]
11. Rankin EB, Fuh KC, Castellini L, Viswanathan K, Finger EC, Diep AN, et al. Direct regulation of GAS6/AXL signaling by HIF promotes renal metastasis through SRC and MET. Proceedings of the National Academy of Sciences of the United States of America 2014;111:13373–8. [PubMed: 25187556]
12. Gustafsson A, Bostrom AK, Ljungberg B, Axelson H, Dahlback B. Gas6 and the receptor tyrosine kinase Axl in clear cell renal cell carcinoma. PloS one 2009;4:e7575. [PubMed: 19888345]
13. Gustafsson A, Martuszewska D, Johansson M, Ekman C, Hafizi S, Ljungberg B, et al. Differential expression of Axl and Gas6 in renal cell carcinoma reflecting tumor advancement and survival. Clinical cancer research : an official journal of the American Association for Cancer Research 2009;15:4742–9. [PubMed: 19567592]
14. Zhou L, Liu XD, Sun M, Zhang X, German P, Bai S, et al. Targeting MET and AXL overcomes resistance to sunitinib therapy in renal cell carcinoma. Oncogene 2016;35:2687–97. [PubMed: 26364599]
15. Linger RM, Keating AK, Earp HS, Graham DK. Taking aim at Mer and Axl receptor tyrosine kinases as novel therapeutic targets in solid tumors. Expert Opin Ther Targets 2010;14:1073–90. [PubMed: 20809868]
16. Karam JA, Zhang XY, Tamboli P, Margulis V, Wang H, Abel EJ, et al. Development and characterization of clinically relevant tumor models from patients with renal cell carcinoma. Eur Urol 2011;59:619–28. [PubMed: 21167632]
17. Cerami E, Gao J, Dogrusoz U, Gross BE, Sumer SO, Aksoy BA, et al. The cBio cancer genomics portal: an open platform for exploring multidimensional cancer genomics data. Cancer discovery 2012;2:401–4. [PubMed: 22588877]
18. Wilkerson MD, Hayes DN. ConsensusClusterPlus: a class discovery tool with confidence assessments and item tracking. Bioinformatics 2010;26:1572–3. [PubMed: 20427518]
19. Kariolis MS, Miao YR, Diep A, Nash SE, Olcina MM, Jiang D, et al. Inhibition of the GAS6/AXL pathway augments the efficacy of chemotherapies. The Journal of clinical investigation 2017;127:183–98. [PubMed: 27893463]
20. Bydoun M, Sterea A, Weaver ICG, Bharadwaj AD, Waisman DM. A novel mechanism of plasminogen activation in epithelial and mesenchymal cells. Scientific reports 2018;8:14091. [PubMed: 30237490]
21. Thong AE, Zhao H, Ingels A, Valta MP, Nolley R, Santos J, et al. Tissue slice grafts of human renal cell carcinoma: an authentic preclinical model with high engraftment rate and metastatic potential. Urologic oncology 2014;32:43 e23–30.

22. Palisoul ML, Quinn JM, Schepers E, Hagemann IS, Guo L, Reger K, et al. Inhibition of the Receptor Tyrosine Kinase AXL Restores Paclitaxel Chemosensitivity in Uterine Serous Cancer. Molecular cancer therapeutics 2017;16:2881–91. [PubMed: 28904132]
23. Kumari S, Malla R. New Insight on the Role of Plasminogen Receptor in Cancer Progression. Cancer growth and metastasis 2015;8:35–42. [PubMed: 26279629]
24. Surette AP, Madureira PA, Phipps KD, Miller VA, Svenningsson P, Waisman DM. Regulation of fibrinolysis by S100A10 in vivo. Blood 2011;118:3172–81. [PubMed: 21768297]
25. Ling Q, Jacovina AT, Deora A, Febbraio M, Simantov R, Silverstein RL, et al. Annexin II regulates fibrin homeostasis and neoangiogenesis in vivo. The Journal of clinical investigation 2004;113:38–48. [PubMed: 14702107]
26. Madureira PA, O'Connell PA, Surette AP, Miller VA, Waisman DM. The biochemistry and regulation of S100A10: a multifunctional plasminogen receptor involved in oncogenesis. Journal of biomedicine & biotechnology 2012;2012:353687. [PubMed: 23118506]
27. Liu W, Hajjar KA. The annexin A2 system and angiogenesis. Biological chemistry 2016;397:1005–16. [PubMed: 27366903]
28. Ferrara N Binding to the extracellular matrix and proteolytic processing: two key mechanisms regulating vascular endothelial growth factor action. Molecular biology of the cell 2010;21:687–90. [PubMed: 20185770]
29. Potente M, Gerhardt H, Carmeliet P. Basic and therapeutic aspects of angiogenesis. Cell 2011;146:873–87. [PubMed: 21925313]
30. Nowak-Sliwinska P, Alitalo K, Allen E, Anisimov A, Aplin AC, Auerbach R, et al. Consensus guidelines for the use and interpretation of angiogenesis assays. Angiogenesis 2018;21:425–532. [PubMed: 29766399]
31. Choueiri TK, Halabi S, Sanford BL, Hahn O, Michaelson MD, Walsh MK, et al. Cabozantinib Versus Sunitinib As Initial Targeted Therapy for Patients With Metastatic Renal Cell Carcinoma of Poor or Intermediate Risk: The Alliance A031203 CABOSUN Trial. Journal of clinical oncology : official journal of the American Society of Clinical Oncology 2017;35:591–7. [PubMed: 28199818]
32. Yakes FM, Chen J, Tan J, Yamaguchi K, Shi Y, Yu P, et al. Cabozantinib (XL184), a novel MET and VEGFR2 inhibitor, simultaneously suppresses metastasis, angiogenesis, and tumor growth. Molecular cancer therapeutics 2011;10:2298–308. [PubMed: 21926191]
33. Truong LD, Shen SS. Immunohistochemical diagnosis of renal neoplasms. Archives of pathology & laboratory medicine 2011;135:92–109. [PubMed: 21204715]
34. Holland SJ, Pan A, Franci C, Hu Y, Chang B, Li W, et al. R428, a selective small molecule inhibitor of Axl kinase, blocks tumor spread and prolongs survival in models of metastatic breast cancer. Cancer research 2010;70:1544–54. [PubMed: 20145120]
35. Holland SJ, Powell MJ, Franci C, Chan EW, Friera AM, Atchison RE, et al. Multiple roles for the receptor tyrosine kinase axl in tumor formation. Cancer research 2005;65:9294–303. [PubMed: 16230391]
36. Li Y, Ye X, Tan C, Hongo JA, Zha J, Liu J, et al. Axl as a potential therapeutic target in cancer: role of Axl in tumor growth, metastasis and angiogenesis. Oncogene 2009
37. Ye X, Li Y, Stawicki S, Couto S, Eastham-Anderson J, Kallop D, et al. An anti-Axl monoclonal antibody attenuates xenograft tumor growth and enhances the effect of multiple anticancer therapies. Oncogene 2010;29:5254–64. [PubMed: 20603615]
38. Ruan GX, Kazlauskas A. Axl is essential for VEGF-A-dependent activation of PI3K/Akt. The EMBO journal 2012;31:1692–703. [PubMed: 22327215]
39. O'Connell PA, Surette AP, Liwski RS, Svenningsson P, Waisman DM. S100A10 regulates plasminogen-dependent macrophage invasion. Blood 2010;116:1136–46. [PubMed: 20424186]
40. Phipps KD, Surette AP, O'Connell PA, Waisman DM. Plasminogen receptor S100A10 is essential for the migration of tumor-promoting macrophages into tumor sites. Cancer research 2011;71:6676–83. [PubMed: 22042827]
41. Noye TM, Lokman NA, Oehler MK, Ricciardelli C. S100A10 and Cancer Hallmarks: Structure, Functions, and its Emerging Role in Ovarian Cancer. International journal of molecular sciences 2018;19

42. Domoto T, Miyama Y, Suzuki H, Teratani T, Arai K, Sugiyama T, et al. Evaluation of S100A10, annexin II and B-FABP expression as markers for renal cell carcinoma. Cancer science 2007;98:77–82. [PubMed: 17083565]

43. Teratani T, Watanabe T, Kuwahara F, Kumagai H, Kobayashi S, Aoki U, et al. Induced transcriptional expression of calcium-binding protein S100A1 and S100A10 genes in human renal cell carcinoma. Cancer letters 2002;175:71–7. [PubMed: 11734338]

44. Ricketts CJ, Crooks DR, Linehan WM. Targeting HIF2alpha in Clear-Cell Renal Cell Carcinoma. Cancer cell 2016;30:515–7. [PubMed: 27728802]

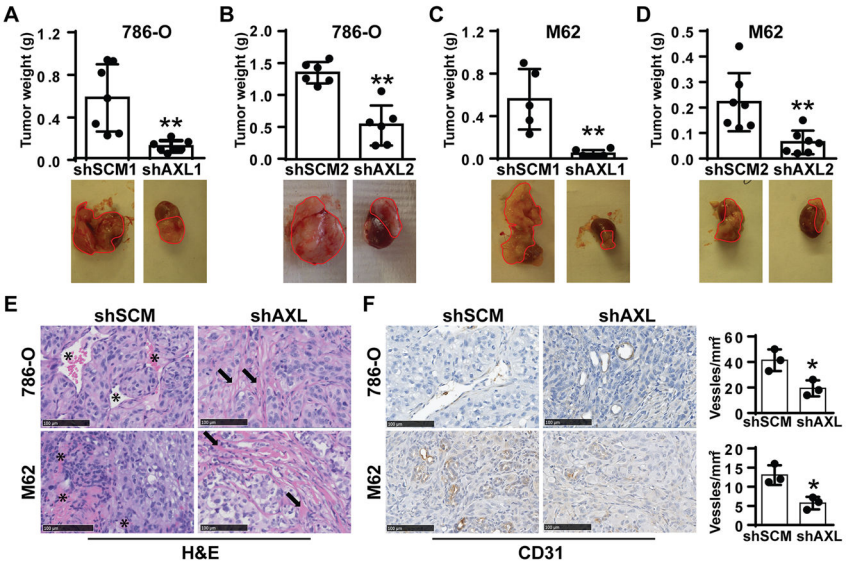

Fig. 1. Genetic inactivation of AXL is sufficient to reduce ccRCC orthotopic tumor growth and vessel density in the renal capsule.

(A) Total tumor weight (upper, n=7) and macroscopic picture (lower) of primary tumors taken from mice orthotopic sub-renal capsule injection of shSCM1 or shAXL1 786-O cells. (B) Total weight (upper, n=6) and macroscopic picture (lower) of primary tumors taken from mice orthotopic sub-renal capsule injection of shSCM2 or shAXL2 786-O cells. (C) Total weight (upper, n=5 for shSCM1 and n=6 for shAXL1) and macroscopic picture (lower) of primary tumors taken from mice orthotopic sub-renal capsule injection of shSCM1 or shAXL1 M62 cells. (D) Total weight (upper, n=7) and macroscopic picture (lower) of primary tumors taken from mice orthotopic sub-renal capsule injection of shSCM2 or shAXL2 M62 cells. (E) Hematoxylin and eosin staining (H&E) of primary tumors taken from mice orthotopic sub-renal capsule injection of shSCM or shAXL 786-O (upper) and M62 (lower) cells. The "*" indicates blood vessel and the arrow indicates extracellular matrix. (F) CD31 staining (left) and blood vessel number (right) of primary tumors taken from mice orthotopic sub-renal capsule injection of shSCM or shAXL 786-O (upper) and M62 (lower) cells (three mice, five fields per tumor). Data represent the averages ± SD. *$p < 0.05$ and **$p < 0.01$.

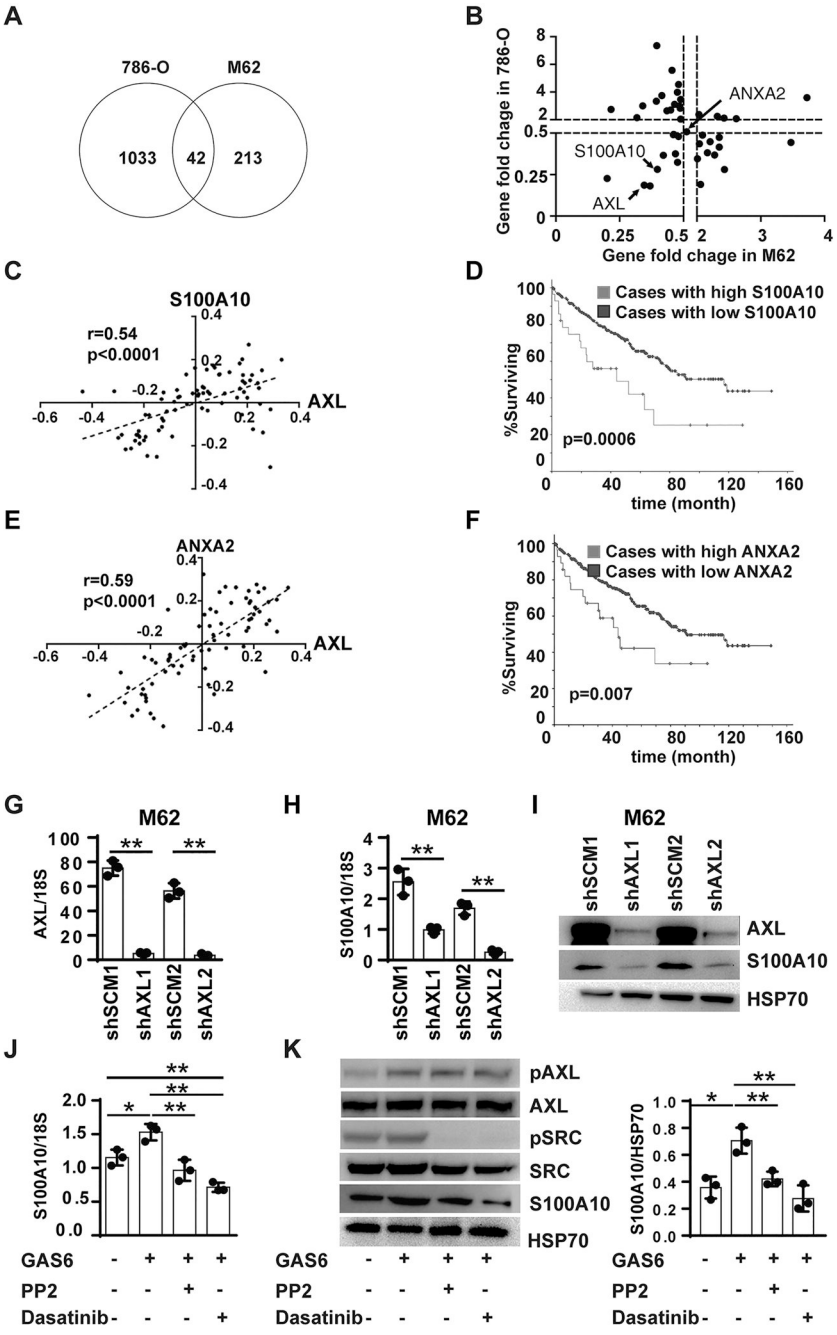

Fig. 2. GAS6/AXL signaling promotes S100A10 expression in ccRCC cells.

(A) Venn diagram showing the number of genes that have >2-fold change in 786-O and M62 cells with AXL knockdown. Forty-two genes have >2-fold change in both 786-O and M62 AXL knockdown cells. (B) Scatter plot showing the gene fold change of the forty-two genes with >2-fold change in 786-O and M62 cells. Arrows point to *AXL*, *S100A10* and *ANXA2*. (C) Correlation of *AXL* and *S100A10* transcript levels in 76 ccRCC patient samples from Gene Expression Onmbus (GEO) (GSE36985). (D) Kaplan-Meier survival analysis based on *S100A10* mRNA levels in 538 ccRCC patients from TCGA. (E) Correlation of transcript levels of *ANXA2* and *AXL* in 76 ccRCC patient samples from Gene Expression Onmbus

(GEO) (GSE36985). (F) Kaplan-Meier survival analysis based on *ANXA2* mRNA levels in 538 ccRCC patients from TCGA. (G-H) Real-time PCR analysis of *AXL* (G) and *S100A10* (H) expression in the M62 cells transfected with shSCM1, shAXL1, shSCM2 or shAXL2. (I) Western blot analysis of AXL and S100A10 expression in shSCM1, shAXL1, shSCM2 or shAXL2 M62 cells. HSP70 was used as loading control. (J) Real-time PCR analysis of serum-starved M62 cells treated with either GAS6 (200 ng/mL) alone or in combination with SRC inhibitors PP2 (500 nM) or dasatinib (50 nM). (K) Representative western blot (left) and quantification of S100A10 (right) in serum-starved M62 cells treated with either GAS6 (200 ng/mL) alone or in combination with SRC inhibitors PP2 (500 nM) or dasatinib (50 nM). HSP70 was used as loading control. All experiments were independently repeated three times. Data represent the averages ± SD. *$p < 0.05$ and **$p < 0.01$.

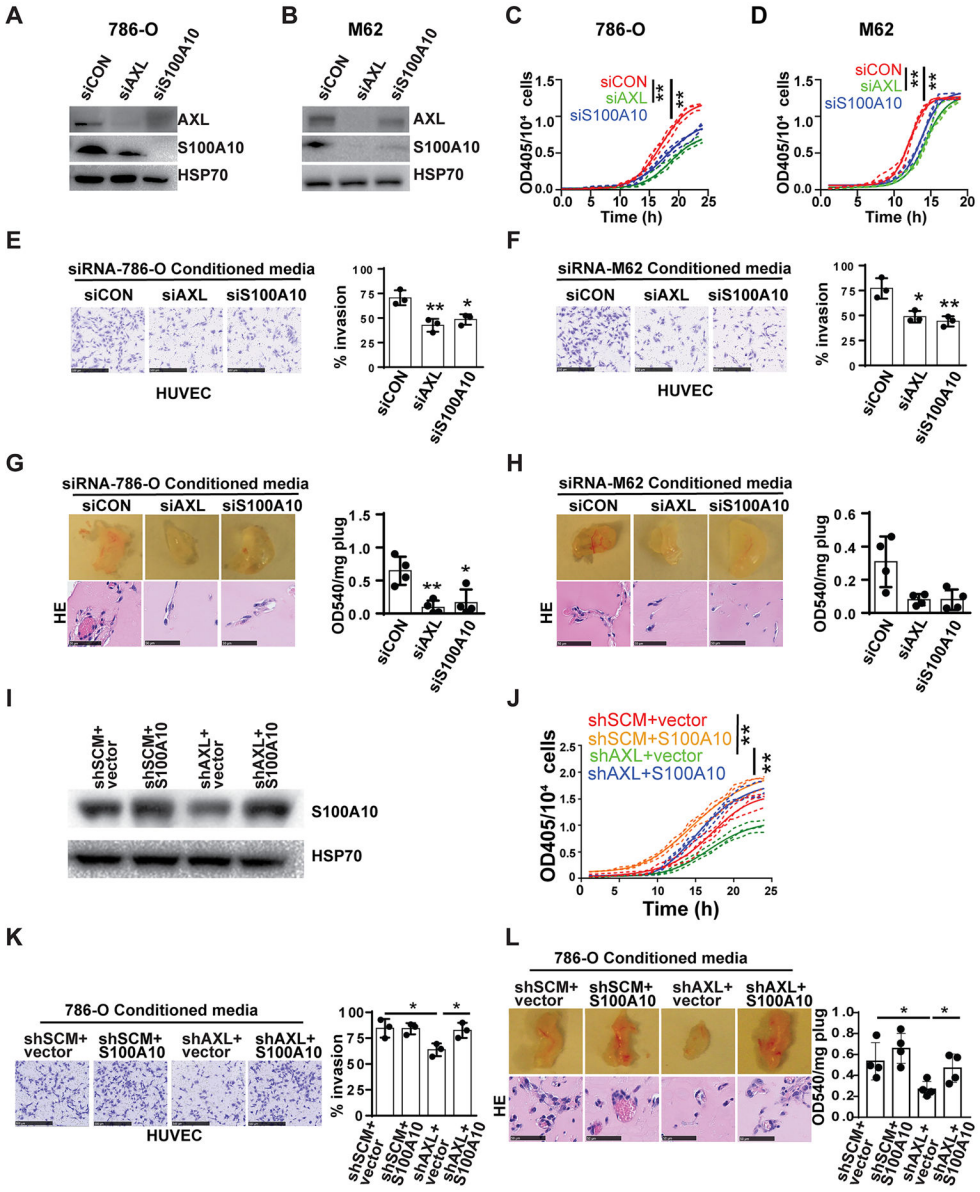

Fig. 3. AXL and S100A10 promote the angiogenic potential of ccRCC cells in vitro and in vivo.

(A-B) Western blot analysis of AXL and S100A10 expression in 786-O (A) and M62 (B) cells transfected with siCON, siAXL or siS100A10 siRNA pools. HSP70 was used as a loading control. (C-D) The rate of plasmin generation in 786-O (C) or M62 (D) cells transfected with siCON, siAXL or siS100A10. Solid lines indicate the average and dashed lines indicate the variance. (E-F) Representative pictures (left) and the invasion ratio (right) of HUVEC cells invaded through Matrigel coated membranes primed with cell culture supernatants derived from 786-O (E) and M62 (F) cells transfected with siCON, siAXL or siS100A10. (G-H) Macroscopic pictures (top left), H&E staining (bottom left) and quantification of hemoglobin (right) in matrigel plugs taken from mice 10 days following s.c. injection of matrigel mixed with cell culture supernatant derived from 786-O (G) and M62 (H) cells transfected with siCON, siAXL or siS100A10. Results represent the ratio of

OD540 to the weight of plus used for hemoglobin quantification. (I) Western blot analysis of S100A10 expression in cell 786-O-shSCM and shAXL cells transfected with empty vector or S100A10 overexpression vector. HSP70 was used as a loading control. (J) The rate of plasmin generation in cell 786-O-shSCM and shAXL cells transfected with empty vector or S100A10 overexpression vector. (K) Representative pictures (left) and the invasion ratio (right) of HUVEC cells invaded through matrigel coated membranes primed with cell culture supernatants derived from 786-O shSCM and shAXL cells transfected with empty vector or S100A10 expression vector. (L) Macroscopic pictures (top left), H&E staining (bottom left) of the matrigel plugs and quantification of the hemoglobin (right) in matrigel plugs taken from mice 10 days following s.c. injection of matrigel mixed with cell culture supernatant derived from 786-O shSCM and shAXL cells transfected with empty vector or S100A10 expression vector. Data represent the averages ± SD. Experiments were independently repeated three times. Error bars represent ±SD. *$p < 0.05$ and **$p < 0.01$.

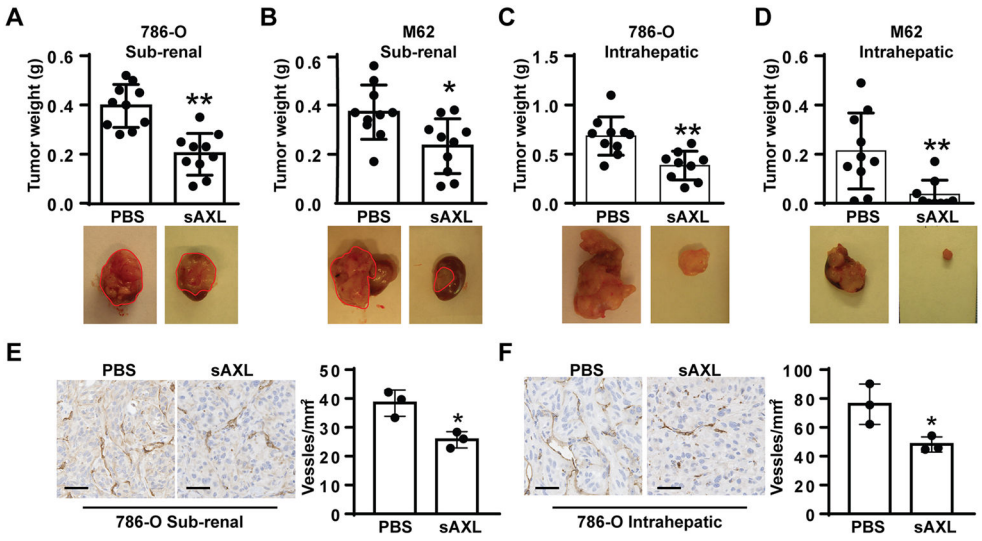

Fig. 4. Soluble AXL (sAXL) therapy inhibits ccRCC tumor growth and vessel density.

(A-B) Total weight (upper, n=10) and macroscopic picture (lower) of primary tumors taken from mice orthotopic sub-renal capsule injection of parental 786-O (A) and M62 (B) cells treated with PBS or sAXL (20 mg/kg, every two days). (C-D) Total weight (upper, n=10 for PBS and n=9 for sAXL) and macroscopic picture (lower) of tumors taken from mice intrahepatic injection of parental 786-O (C) and M62 (D) cells treated with PBS or sAXL. (E) CD31 staining (left) and blood vessel number (right) of primary tumors taken from mice orthotopic sub-renal capsule injection of 786-O cells post treated with PBS or sAXL (three mice, five fields per tumor). Data represent the averages ± SD. *$p < 0.05$ and **$p < 0.01$. (F) CD31 staining (left) and blood vessel number (right) of primary tumors taken from mice intrahepatic injection of 786-O cells post treated with PBS or sAXL (three mice, five fields per tumor) Data represent the averages ± SD. *$p < 0.05$ and **$p < 0.01$.

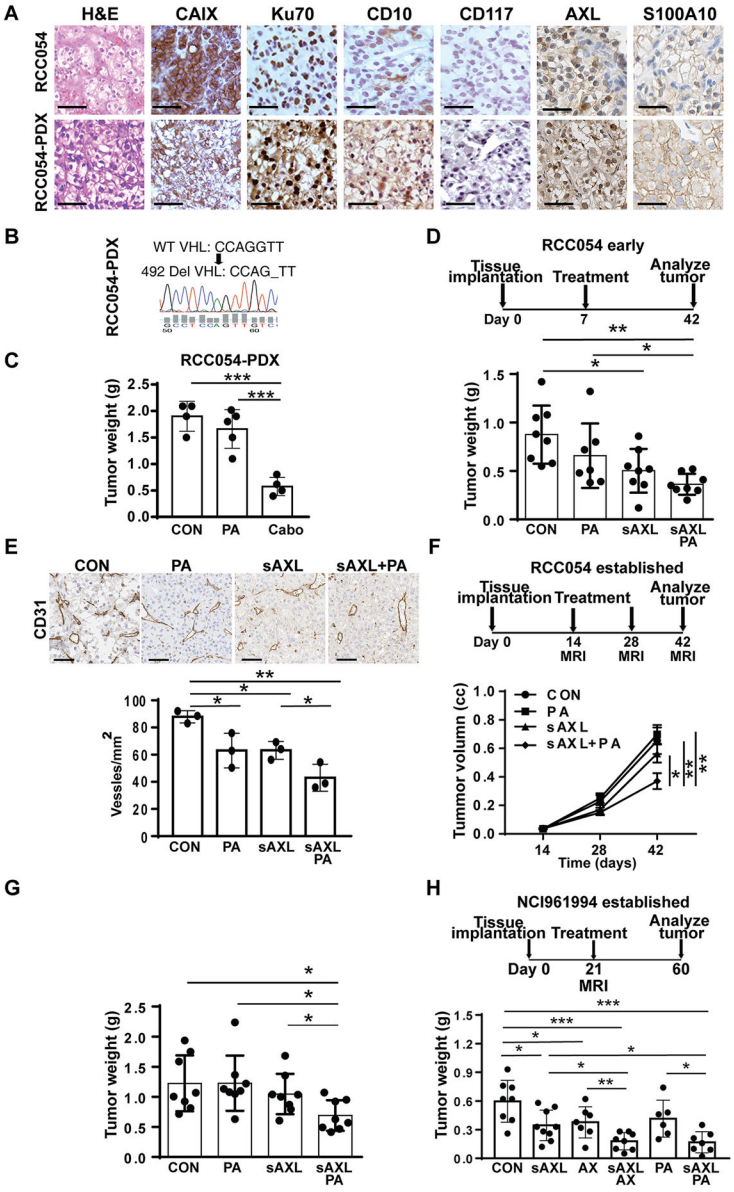

Fig. 5. AXL inhibitors synergize with anti-angiogenic therapy to inhibit ccRCC PDX tumor growth.

(A) H&E and IHC staining of CAIX, Ku70, CD10, CD117, AXL and S100A10 within the primary patient (*upper*) and PDX (*lower*) tissue. (B) Sequencing of VHL in RCC054-PDX tumor showing a VHL deletion mutation at nucleotide 492. (C) Total tumor weights of RCC054 PDX treated with pazopanib (PA) or cabozantinib. (D) Schematic description of sAXL and pazopanib (PA) for early RCC054-PDX treatment scheduling (*upper*) and tumor weight (*lower*). (E) CD31 staining (*upper*) and blood vessel number (*lower*) of PDX tumors taken from mice treated with sAXL, pazopanib (PA) or combo (sAXL+PA) (three mice, ten fields per tumor). (F) Schematic description of sAXL and pazopanib (PA) for established RCC054-PDX treatment scheduling (*upper*) and tumor growth curve (*lower*). (G) Total tumor weights of RCC054 established study in (F) at the endpoint analysis. (H) Schematic description of sAXL, axitinib (AX) and pazopanib (PA) for established NCI961994-PDX

treatment scheduling (*upper*) and tumor weight (*lower*). Data represent the averages ± SD. *p < 0.05, **p < 0.01 and ***p < 0.001.